Journal of Materials Chemistry A

ROYAL SOCIETY OF CHEMISTRY

PAPER

View Article Online
View Journal | View Issue

Cite this: J. Mater. Chem. A, 2023, 11, 9538

Achieving high performance organic solar cells with a closer π−π distance in branched alkyl-chain acceptors†

Pu Tan,‡[a] Congcong Cao,‡[a] Yue Cheng,‡[a] Hui Chen,[a] Hanjian Lai,[a] Yulin Zhu,[ab] Liang Han,[a] Jianfei Qu,[a] Nan Zheng,[d] Yuanzhu Zhang [a] and Feng He *[ac]

Received 20th February 2023
Accepted 27th March 2023

DOI: 10.1039/d3ta01049j

rsc.li/materials-a

Side-chain functional groups have been shown to not only ensure solubility but also influence molecular packing behavior, and side-chain modification is an important strategy in the optimization of photovoltaic performance. Instead of focusing on the size of the alkyl side chains, we have investigated the influence of side-chain configurations on the properties of acceptors and organic solar cells (OSCs). Two acceptor molecules, **BTIC-TCl-*b*** and **BTIC-TCl-*l*** were designed by changing the linear configuration of alkyl chain substituents on thiophene rings to a branched structure. The results show that the branched configuration of the side-chain can significantly improve the planarity and reduce the π···π distances, leading to a more compact 3D-network structure. With the polymer donor PBDB-TF, an outstanding power conversion efficiency (PCE) of 16.17% was achieved by **BTIC-TCl-*b***, which is significantly higher than that found with **BTIC-TCl-*l***. Our study offers new insights for side-chain modification, regulation of the aggregation state, and optimization of photovoltaic performance.

Introduction

Organic solar cells (OSCs) with the advantages of flexibility, transparency, and roll-to-roll production have in recent decades, become an effective supplement to silicon-based solar cells.[1–4] The OSC research community has made great efforts to modify the characteristics of materials used in active layers to obtain better properties.[5–8] Since the paradigm shift from the ITIC-series[9] to the Y6-series,[10] the 18% PCE of devices based on bulk-heterojunctions[11–17] or quasi-planar heterojunctions[8,18,19] has been surpassed by the state-of-the-art non-fullerene acceptors (NFAs).[20,21] This exceptional improvement in OSC devices can be attributed to the design of the donor and acceptor materials, the proper application and understanding of molecular interactions,[8,22–25] the charge dynamics[26,27] and the processes for the preparation of devices. At present, the main problem in the industrial production of OSCs is whether the capabilities of materials and techniques[24,28–30] have been completely developed. As a result, one of the most important items in current research is deep exploration of the potential of OSCs with a view to achieving better performance through the optimization of materials.[31–35]

To achieve ideal charge transportation, the solubility and the interaction of NFA molecules and the morphology[36,37] of blends with donor materials should be maximized for improved photovoltaic properties. From the perspective of molecular design and its modification, changes in the side chains[35,38–41] of acceptors are among the most convenient and efficient methods to regulate the packing modes and solubility of molecules. In previous research, the rational choice of the length,[40] configuration[33,38–41] and substitution position of the side chains that are connected to the pyrrole ring is a key strategy for regulation of molecular aggregation.[35] Generally, longer or larger side chains can lead to a more uniform distribution and avoidance of excessive aggregation of the single donor or acceptor phases, which means the materials will have excellent processability in solution. However, such a single structural change does not ensure the performance improvement expected from the design due to competing effects on device efficiencies. For instance, the use of longer or branched alkyl chains can improve the solubility of the materials, but the accompanying steric effect will weaken the intermolecular interactions and thus reduce the charge mobility of the materials, and this leads to a trade-off between solution-processability and device properties. Among the numerous

[a]Shenzhen Grubbs Institute and Department of Chemistry, Southern University of Science and Technology, Shenzhen 518055, China. E-mail: hef@sustech.edu.cn
[b]School of Chemistry and Chemical Engineering, Harbin Institute of Technology, Harbin, 150001, China
[c]Guangdong Provincial Key Laboratory of Catalytic Chemistry, Southern University of Science and Technology, Shenzhen 518055, China
[d]Institute of Polymer Optoelectronic Materials and Devices, State Key Laboratory of Luminescent Materials and Devices, South China University of Technology, Guangzhou 510640, China

† Electronic supplementary information (ESI) available. CCDC **BTIC-TCl-*b***: 2240315 and **BTIC-TCl-*l***: 2240316. For ESI and crystallographic data in CIF or other electronic format see DOI: https://doi.org/10.1039/d3ta01049j

‡ These authors contributed equally.

studies of alkyl chains in this context, we found that the choice of branched chains connected to the pyrrole ring is preferable on the inner side while the conformation of the alkyl chains on the outer side of the molecule is still open to exploration.[38] For example, when the outer alkyl chain of Y6 had been changed to branched chains in L8-BO,[39] the packing mode of this molecule changed significantly from their single crystals, in which the size of the framework also became small. It indicates that the change of the outer alkyl chain conformation can affect the packing mode of final molecules, but the underlying reason of this effect still needs to be analyzed and further clarified.

With this point of view, we examined the replacement of the linear chains with thiophene groups by alkyl chain substituents on the outside position of the acceptor molecule. Two NFAs, **BTIC-TCl-*b*** and **BTIC-TCl-*l*** were designed and synthesized with different alkyl configurations of branched and linear chains. **BTIC-TCl-*b*** and **BTIC-TCl-*l*** have a similar V_{OC} of 0.88 V and the structure and property effects caused by the configuration differences were systematically investigated. Combined with the V_{OC}, a slightly red-shifted absorption of **BTIC-TCl-*b*** caused an enhanced J_{SC} and afforded **BTIC-TCl-*b*** the highest PCE of 16.17%. Single-crystal analysis showed that despite their slight structural differences in the alkyl chain configuration, the two NFAs were packed quite differently. We found that in systems containing both molecules, only **BTIC-TCl-*b*** with branched side chains can form 3D stacks to provide multi-channel electron transport. The significantly shortened π···π distance and smaller channel size of **BTIC-TCl-*b*** make it the best performer in the photovoltaic performance. Consequently, the use of the side-chain branching structural design for NFAs may prove to be a promising strategy toward multi-channel exciton transport and performance enhancement of OSCs.

Results and discussion

The chemical structures of **BTIC-TCl-*b*** and **BTIC-TCl-*l*** are shown in Fig. 1, and their synthesis methods and structural characterization are shown in Scheme S1 and Fig. S2–S5 in the ESI.† For the production of two molecules with different side chain configurations, the synthesis began with 4-chloro-2-(2-ethylhexyl)thiophene (TCl-*b*) or 4-chloro-2-octylthiophene (TCl-*l*), which represent straight and branch chains, respectively. After a Stile coupling reaction with 3-bromothieno[3,2-*b*]thiophene, two monomers that were used to prepare the central cores of **BTIC-TCl-*b*** and **BTIC-TCl-*l*** were synthesized. The synthetic methods used to obtain the final products have been reported previously.[38] The branched alkyl chains equip **BTIC-TCl-*b*** with better solubility than **BTIC-TCl-*l***, but both NFAs can dissolve readily in common organic solvents, such as chloroform, dichloromethane, THF, and chlorobenzene. Differential scanning calorimetry (DSC) and thermogravimetric analysis (TGA) were used to measure the thermal properties of **BTIC-TCl-*b*** and **BTIC-TCl-*l***, and the corresponding curves are shown in Fig. S1.† Both **BTIC-TCl-*b*** and **BTIC-TCl-*l*** show good thermal stability, with 5%-weight-loss temperatures (T_d) of 336 and 317 °C, respectively, and with no obvious peak observed in the DSC traces, both molecules meet the thermal requirements as acceptors in active layers of OSC devices.

UV-Vis absorption was employed to characterize the photoelectric properties of **BTIC-TCl-*b*** and **BTIC-TCl-*l***, and the obtained spectra are shown in Fig. 1. The almost identical response in the range of 400–1000 nm of the two NFAs in the absorption spectra is shown in Fig. 1e and f, and the maximum absorption peaks in the film state are at 828 nm and 823 nm for **BTIC-TCl-*b*** and **BTIC-TCl-*l***, respectively, which show a red-shift of about 90 nm when compared to the absorption in a chloroform solution. The difference in the maximum absorption peaks of **BTIC-TCl-*b*** and **BTIC-TCl-*l*** indicates that the configuration of the alkyl chains contributes to the influence of conjugated or inductive effects, in both branched and linear structures, and has a characteristic impact on the electronic structure of the molecular backbone. The absorption onset of the two NFAs is located at 912 nm in **BTIC-TCl-*b*** and 904 nm in **BTIC-TCl-*l***, which corresponds to optical bandgaps (E_g) of 1.36 eV and 1.37 eV, respectively. By comparing the absorption behavior of the two materials in solution and in a film, we can hypothesize that changes in alkyl chain conformation affect the aggregation mode of molecules and intermolecular electronic coupling, as well as the energy gap between the highest occupied molecular orbital (HOMO) and the lowest unoccupied molecular orbital (LUMO). For further exploration, cyclic voltammetry (CV) was employed to estimate the energy levels of **BTIC-TCl-*b*** and **BTIC-TCl-*l***. The LUMO/HOMO energy levels of **BTIC-TCl-*b***, **BTIC-TCl-*l***, and PBDB-TF are −3.90/−5.70 eV, −3.92/−5.75 eV, and −3.65/−5.45 eV respectively, as shown in Fig. 1g, and the electrochemical bandgaps of **BTIC-TCl-*b*** and **BTIC-TCl-*l*** based on the tests are 1.80 and 1.83 eV, respectively. The difference between these corresponds to the optical bandgaps (E_g).

It is widely recognized that aggregation behavior affects many properties of materials in the blend film, including intermolecular electron coupling, UV absorption, distribution of energy levels, solubility, mobility, and phase separation. Consequently, a study based on molecular packing patterns is necessary to explain the difference in the photovoltaic properties of materials. Crystals of **BTIC-TCl-*b*** and **BTIC-TCl-*l*** were produced by solvent precipitation for 1 or 2 weeks at room temperature and their crystallographic data were collected from X-ray single crystal diffraction. This single-crystal information can be found in the Cambridge Crystallographic Data Centre, where the CCDC numbers of **BTIC-TCl-*b*** and **BTIC-TCl-*l*** are 2240315 and 2240316, respectively. As shown in Fig. 1c and d, the two NFAs present classical configurations of Y-series NFA molecules locked by non-covalent interactions of S···O with distances of 2.63 and 2.66 Å, respectively. Significantly, **BTIC-TCl-*b*** not only has shorter S···O distances but also exhibits smaller dihedral angles of 43.19° and 5.66°, while **BTIC-TCl-*l*** with dihedral angles of 43.60° and 8.53° suggests that **BTIC-TCl-*b*** has better planarity of the two molecules. Meanwhile, S···S interactions were formed between the side chain thiophene ring and the backbone with distances of 3.37 and 3.40 Å, respectively, which is consistent with the planarity changes in **BTIC-TCl-*b*** and **BTIC-TCl-*l***. The single molecular crystal nature of

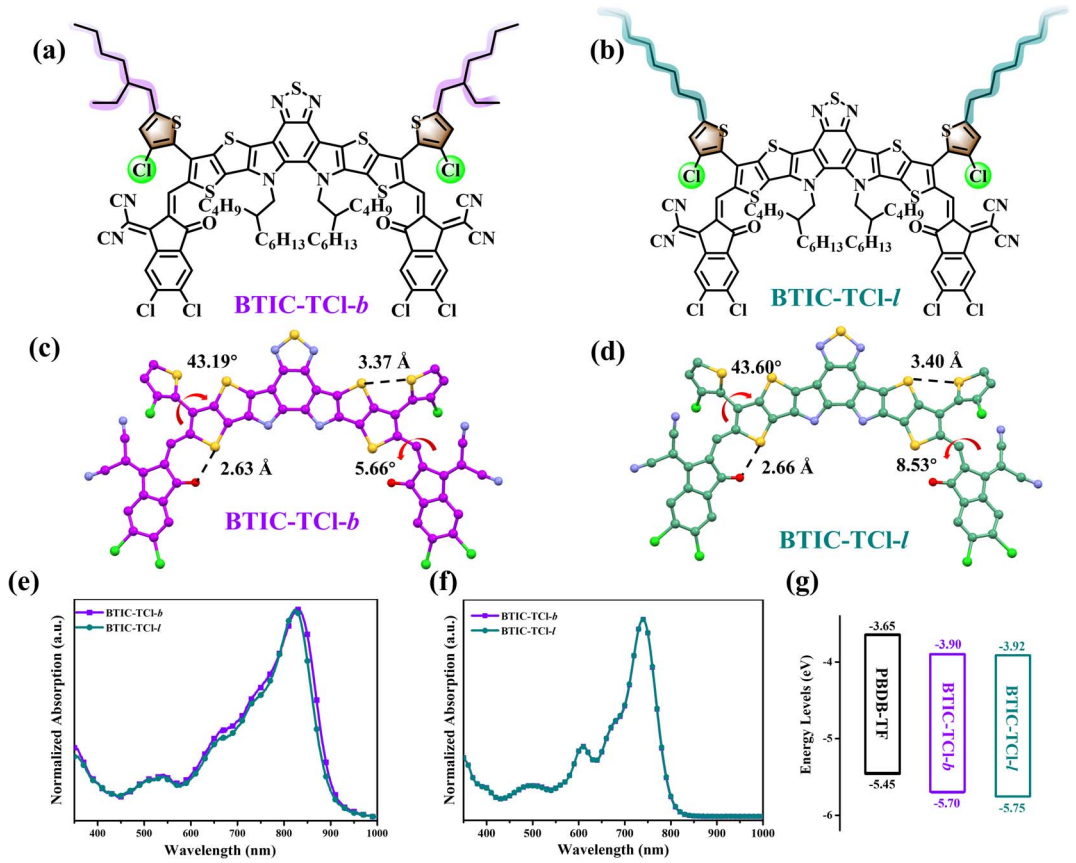

Fig. 1 The structures of (a) BTIC-TCl-***b*** and (b) BTIC-TCl-***l***. The single crystal structures of (c) BTIC-TCl-***b*** and (d) BTIC-TCl-***l***. The UV-Vis absorption spectra of the two materials in (e) films and (f) chloroform. (g) The LUMO/HOMO energy levels of the two acceptors and PBDB-TF.

BTIC-TCl-*b* suggests that it will be more conducive to the packing of the molecules.

Through the single crystal analysis, it was found that the molecular packing of **BTIC-TCl-*b*** and **BTIC-TCl-*l*** is composed of three kinds of basic states including the intermolecular interaction between the core and terminal group (CT), the intermolecular interaction between terminal groups with the opposite molecular orientation (TT-1), and the intermolecular interaction between terminal groups with the same molecular orientation mode (TT-2), respectively. As shown in Fig. 2a and b, the π⋯π distances of two packing states in **BTIC-TCl-*b*** are 3.40 Å in the CT mode and 2.98 Å in the TT-1 mode, and in **BTIC-TCl-*l*** are 3.65 Å in the CT mode and 3.58 Å in the TT-2 mode. **BTIC-TCl-*b*** has significantly shorter π⋯π distances than **BTIC-TCl-*l***, and this underlies the superior molecular planarity of **BTIC-TCl-*b*** which will facilitate intermolecular charge transfer.

The aggregation states of **BTIC-TCl-*b*** and **BTIC-TCl-*l*** are analyzed in Fig. 3a–d. Both acceptors can form framework structures with four adjacent molecules through non-covalent bonding, while there are some differences in the intermolecular interactions. As shown in Fig. 3a and c, there are only intermolecular π⋯π and intermolecular S⋯O interactions (3.47 Å) in one framework in **BTIC-TCl-*b***, and benefiting from the reverse aggregation of two molecules in the TT-1 mode, the frameworks can be connected by π⋯π interactions. On the other hand, the chlorine atom in the side-chain thiophene of **BTIC-TCl-*l*** leads to an intermolecular Cl⋯S (3.56 Å) interaction which together with π⋯π interactions can form a framework structure. Different from the TT-1 mode, the TT-2 mode formed by the interaction of codirectional molecules in **BTIC-TCl-*l*** results in the framework not being fully connected by π⋯π interactions but rather by an S⋯S (3.56 Å) interaction, as shown in Fig. 3b and d. As a result, **BTIC-TCl-*b*** shows a 3D network packing structure with a smaller framework in which $L_x = 14.12$ Å (major axis) and $L_y = 13.31$ Å (minor axis) due to its better planarity and CT/TT-1 mode intermolecular interactions. **BTIC-TCl-*l*** on the other hand exhibits a larger framework with $L_x = 14.45$ Å and $L_y = 13.88$ Å and forms a quasi-3D network. The tighter aggregation state of **BTIC-TCl-*b*** provides more possible channels for electron hopping. At this stage, the structure and the size of the 3D/quasi-3D framework can be adjusted by the configuration of the alkyl chain substituents on the thiophene side-chains. This will control the overlap ranges and the number of intermolecular junctions.

To further explore the influence of different alkyl chain configurations on material photovoltaic properties, the conventional structure of ITO/PEDOT:PPS/PBDB-TF:acceptors/PDINO/Ag was synthesized and the photovoltaic performances of OSCs based on **BTIC-TCl-*b*** and **BTIC-TCl-*l*** were examined. The assessment results are shown in Fig. 4a–f, and the

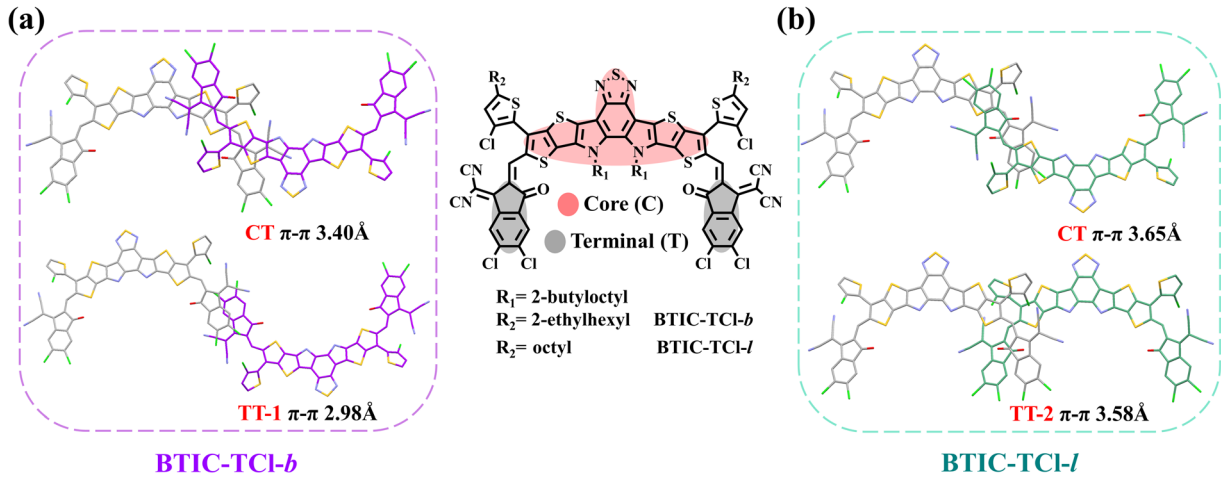

Fig. 2 The different packing modes analyzed using single-crystal data and the corresponding binding energies for (a) BTIC-TCl-*b* and (b) BTIC-TCl-*l*.

corresponding data are summarized in Table 1. The highest PCE of 16.17% is achieved by **BTIC-TCl-*b***-based OSC devices, while the PCE of 15.49% is shown by **BTIC-TCl-*l***-based devices. Both **BTIC-TCl-*b*** and **BTIC-TCl-*l***-based devices show the same V_{OC} of 0.88 V, the difference in PCE mainly came from J_{SC} and FF% of 24.29 mA cm^{-2}/75.78% and 23.84 mA cm^{-2}/73.62%, respectively. From the point of view of the property parameters discussed above, the best photovoltaic performances can be obtained when the configuration of alkyl chains is branched, as in **BTIC-TCl-*b***. It can be seen that when the alkyl chain

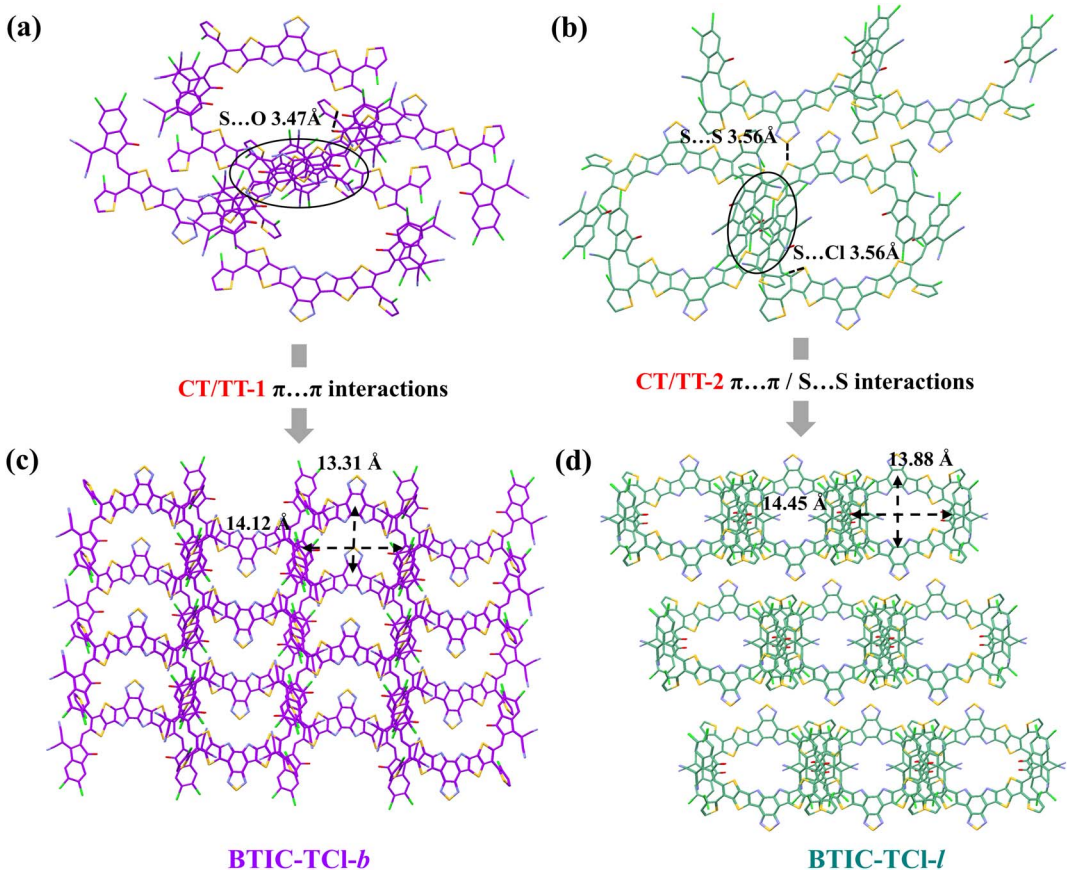

Fig. 3 The intermolecular interactions and aggregation behaviors calculated by single-crystal analysis for (a) and (c) BTIC-TCl-*b* and (b) and (d) BTIC-TCl-*l*.

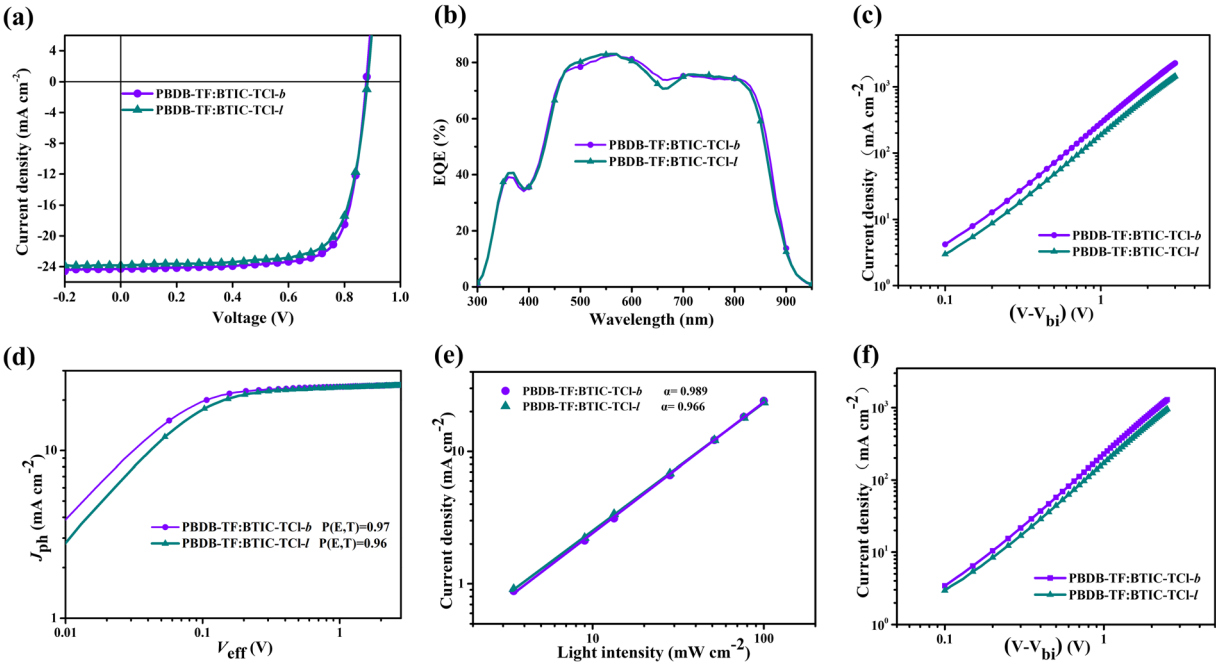

Fig. 4 (a) *J*–*V* curves, (b) EQE curves, (c) the hole mobility curves, (d) Fourier transform photocurrent spectra, (e) bimolecular recombination curves, and (f) the electron mobility curves of devices based on BTIC-TCl-***b*** and BTIC-TCl-***l***.

configuration changes from linear to branched, a PCE improvement occurs in both J_{SC} and FF%. To further understand the origin of the increased J_{SC} in the devices based on **BTIC-TCl-*b*** and **BTIC-TCl-*l***, the external quantum efficiency (EQE) curves of the two NFA-based devices were measured and are shown in Fig. 4b. Both materials have strong light responses in the wavelength range of 450–850 nm, with **BTIC-TCl-*b*** and **BTIC-TCl-*l*** exhibiting more than 70% EQE, indicating that efficient photon–electron conversion occurs in that wavelength range, and **BTIC-TCl-*b*** surpasses this. The calculated currents (J_{cal}) of the two acceptors were obtained by integrating the EQE curves:from the data shown in Table 1, J_{cal} of **BTIC-TCl-*b*** and **BTIC-TCl-*l*** was 23.59 and 23.33 mA cm^{-2}, respectively, matching well with the *J*–*V* tests. The photovoltaic performance calculated based on J_{cal} is shown in Table S1.† To meet the practical application requirements, we prepared OSC devices with an area of 1 cm^2 using the two molecules as the acceptor materials, and the corresponding *J*–*V* and EQE test curves are shown in Fig. S2.† The details are shown in Table S2.†

As discussed above, the packing mode and aggregation behavior lead to effects on exciton mobility that cannot be ignored. This is further reflected in the FF% of the devices based on **BTIC-TCl-*b*** and **BTIC-TCl-*l***. The electron and hole mobility curves were measured by a space-charge-limited-current (SCLC) method, the test results are shown in Fig. 4c and f, and the calculated data are summarized in Table 1. The hole (μ_h) and electron (μ_e) mobility of the two acceptors are significantly different and ascend from **BTIC-TCl-*b*** to **BTIC-TCl-*l*** with 3.9×10^{-4} and 6.4×10^{-4} cm^2 V^{-1} s^{-1} for μ_h, and 3.0×10^{-4} and 5.7×10^{-4} cm^2 V^{-1} s^{-1} for μ_e, respectively. These results are consistent with the difference in PCEs, revealing that the strategies of fixing the alkyl chains at the α-position of the side-chain thiophene rings and changing the configuration to branched are effective in enhancing the charge transport. The higher carrier mobilities of **BTIC-TCl-*b***-based devices benefit from their better molecular packing mode and tighter aggregation as shown by the aforementioned single-crystal analysis, resulting in a higher J_{SC}. The relationship between the photocurrent density (J_{ph}) and the effective voltage (V_{eff}) was investigated in an effort to understand the charge generation and collection properties of the two acceptor-based OSC devices (as in μ_e). The $P_{(E,T)}$ in $P_{(E,T)} = J_{ph}/J_{sat}$ of **BTIC-TCl-*b*** and **BTIC-TCl-*l***-based devices is 0.97 and 0.96, respectively, and **BTIC-TCl-*b*** also has the result closer to 1. We also summarized the relationships between J_{SC} and light intensity (P_{light}) of **BTIC-TCl-*b*** and **BTIC-TCl-*l***-based devices to examine the charge recombination

Table 1 Photovoltaic performance of the two NFA-based OSC devices

Acceptors	V_{OC}[a] (V)	J_{SC}[a] (mA cm^{-2})	FF[a] (%)	PCE$_{max}$[a] (%)	μ_h (cm^2 V^{-1} s^{-1})	μ_e (cm^2 V^{-1} s^{-1})
BTIC-TCl-*b*	0.88 (0.88 ± 0.001)	24.29 (24.15 ± 0.14)	75.78 (75.38 ± 0.40)	16.17 (15.88 ± 0.29)	7.6×10^{-4}	8.7×10^{-4}
BTIC-TCl-*l*	0.88 (0.88 ± 0.001)	23.84 (23.72 ± 0.12)	73.62 (73.07 ± 0.55)	15.49 (15.17 ± 0.32)	5.7×10^{-4}	6.4×10^{-4}

[a] The values in parentheses are average values calculated from 16 devices.

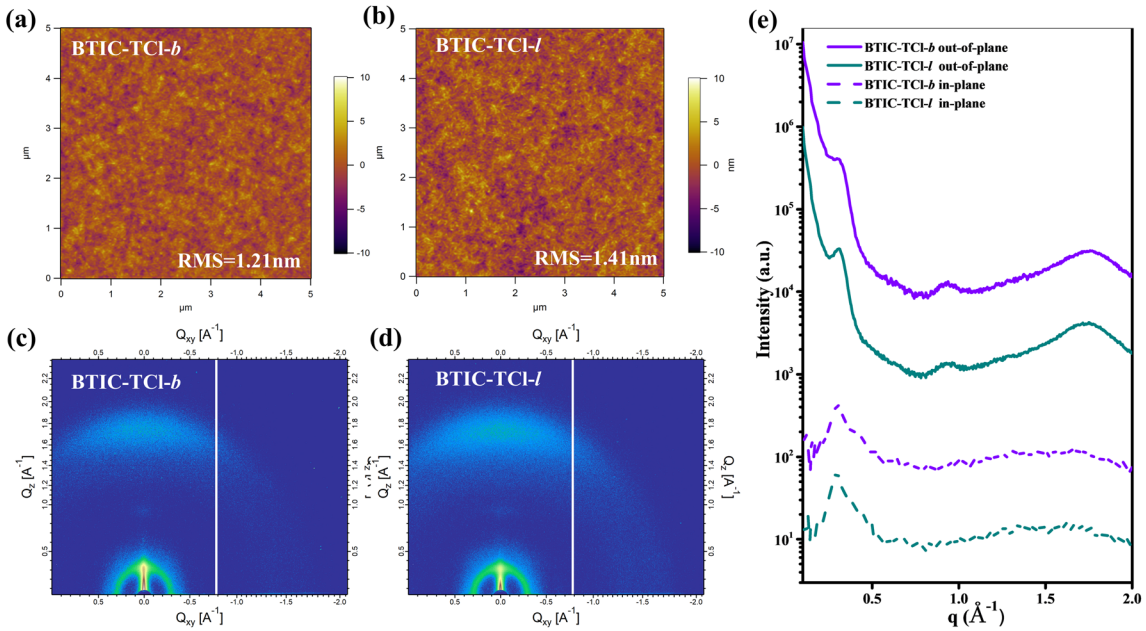

Fig. 5 (a) and (b) The AFM images, (c) and (d) GIWAXS images, and (e) the line-cut profiles of **BTIC-TCl-*b*** and **BTIC-TCl-*l*** blend films with PBDB-TF.

behavior in a short circuit as shown in Fig. 4e. The α in $J_{SC} \propto P_{light}{}^{\alpha}$ of **BTIC-TCl-*b*** is 0.989 which is closer to 1 than in **BTIC-TCl-*l*** ($\alpha = 0.966$). These results indicate that **BTIC-TCl-*b***-based devices have diminished bimolecular recombination, a higher exciton dissociation probability, and better efficient charge collection than **BTIC-TCl-*l***.

Morphology analysis of **BTIC-TCl-*b*** and **BTIC-TCl-*l*** blend films with PBDB-TF was achieved by atomic force microscopy (AFM) and transmission electron microscopy (TEM) measurements to characterize the homogeneity and phase separation of active layer blend films. As displayed in Fig. 5a and b, both **BTIC-TCl-*b*** and **BTIC-TCl-*l***-blend films show uniform surfaces without the formation of undesirably large aggregates, and the root-mean-square (RMS) roughness of **BTIC-TCl-*b*** and **BTIC-TCl-*l***-blend films was found to be ~1.2–1.4 nm, which is conducive to efficient charge dissociation and collection. For further confirmation, TEM was used to capture images for these blend films, and as shown in Fig. S1e and f,† both **BTIC-TCl-*b*** and **BTIC-TCl-*l***-blend films exhibit similar uniform phase distributions. On the other hand, the suitable phase separation sizes of PBDB-TF: **BTIC-TCl-*b*** and PBDB-TF: **BTIC-TCl-*l*** ensured sufficient contact interfaces between the donor and acceptor for efficient separation and transport of excitons, and high J_{SC} and FF% in related devices are guaranteed. The two-dimensional GIWAXS patterns of the blend films are shown in Fig. 5c and d, and the corresponding one-dimensional profiles in the IP and OOP directions are in Fig. 5e. The detailed parameters of 2D-GIWAX profiles are shown in Table S3.† As shown in Fig. 5e and Table S3,† the lamellar diffraction peaks of the two blend films are located at 0.30 and 0.31 $Å^{-1}$, and $\pi\cdots\pi$ stacking diffraction (010) peaks at 1.76 and 1.75 $Å^{-1}$, respectively, with corresponding $\pi\cdots\pi$ distances of 3.55 and 3.59 Å, respectively. It was found that both the blend films of **BTIC-TCl-*b*** and **BTIC-TCl-*l*** with PBDB-TF reflected the predominant face-on orientation, which could improve the transfer of the carriers in the vertical direction, and will be thereby conducive to the photovoltaic properties of the materials.

Conclusions

In summary, two acceptors, **BTIC-TCl-*b*** and **BTIC-TCl-*l*** were designed and synthesized by changing the configurations of the alkyl chains on the side-chain thiophene rings attached to the central core. The impacts of the side-chain configurations on their optoelectronic and molecular aggregation properties were investigated, and it was found that after the configuration of alkyl chains is changed from linear to branched, the planarity of the molecule is enhanced, and the $\pi\cdots\pi$ stacking distance is significantly shortened. The frame size is also reduced, and the packing mode changes from a quasi-3D to a better 3D-network structure. This tightly packed structure formed by changing the alkyl chain configuration enables **BTIC-TCl-*b*** to exhibit enhanced properties of 16.17% in its PCE. Our results indicate that changing the alkyl chain configuration is an effective strategy to enhance the stacking behavior of NFA materials and further improve the photovoltaic performance of the materials.

Data and code availability

The accession number for the single crystal of **BTIC-TCl-*b*** reported in this paper is 2240315 and the accession number for **BTIC-TCl-*l*** is 2240316 in the Cambridge Crystallographic Data Centre (CCDC).

Conflicts of interest

There are no conflicts to declare.

Acknowledgements

This work was financially supported by the National Natural Science Foundation of China (22225504 and 21975115), Shenzhen Fundamental Research Program (JCYJ20200109140801751 and JCYJ20210324120010028), and Guangdong Provincial Key Laboratory of Catalysis (2020B121201002). We also thank the SUSTech Core Research Facilities for the AFM and TEM measurements.

References

1 J. J. M. Halls, C. A. Walsh, N. C. Greenham, E. A. Marseglla, R. H. Frlend, S. C. Morattl and A. B. Holmes, *Nature*, 1995, **376**, 498–500.
2 G. Yu, J. Gao, J. C. Hummelen, F. Wudl and A. J. Heeger, *Science*, 1995, **270**, 1789–1791.
3 G. Li, R. Zhu and Y. Yang, *Nat. Photonics*, 2012, **6**, 153–161.
4 A. J. Heeger, *Adv. Mater.*, 2014, **26**, 10–28.
5 L. Zhu, M. Zhang, J. Xu, C. Li, J. Yan, G. Zhou, W. Zhong, T. Hao, J. Song, X. Xue, Z. Zhou, R. Zeng, H. Zhu, C.-C. Chen, R. C. I. Mackenzie, Y. Zou, J. Nelson, Y. Zhang, Y. Sun and F. Liu, *Nat. Mater.*, 2022, **21**, 656–663.
6 Y. Zou, H. Chen, X. Bi, X. Xu, H. Wang, M. Lin, Z. Ma, M. Zhang, C. Li, X. Wan, G. Long, Y. Zhaoyang and Y. Chen, *Energy Environ. Sci.*, 2022, **15**, 3519–3533.
7 H. Wang, L. Han, J. Zhou, T. Liu, D. Mo, H. Chen, H. Lai, N. Zheng, Z. Xie, W. Zheng and F. He, *CCS Chem.*, 2021, **3**, 2591–2601.
8 H. Lai, X. Lai, Z.-Y. Chen, Y. Zhu, H. Wang, H. Chen, P. Tan, Y. Zhu, Y. Zhang and F. He, *CCS Chem.*, 2022, 1–12.
9 Y. Lin, J. Wang, Z. G. Zhang, H. Bai, Y. Li, D. Zhu and X. Zhan, *Adv. Mater.*, 2015, **27**, 1170–1174.
10 J. Yuan, Y. Zhang, L. Zhou, G. Zhang, H.-L. Yip, T.-K. Lau, X. Lu, C. Zhu, H. Peng, P. A. Johnson, M. Leclerc, Y. Cao, J. Ulanski, Y. Li and Y. Zou, *Joule*, 2019, **3**, 1040–1151.
11 L. Zhu, M. Zhang, J. Xu, C. Li, J. Yan, G. Zhou, W. Zhong, T. Hao, J. Song, X. Xue, Z. Zhou, R. Zeng, H. Zhu, C.-C. Chen, R. C. I. Mackenzie, Y. Zou, J. Nelson, Y. Zhang, Y. Sun and F. Liu, *Nat. Mater.*, 2022, **21**, 656–663.
12 R. Sun, Y. Wu, X. Yang, Y. Gao, Z. Chen, K. Li, J. Qiao, T. Wang, J. Guo, C. Liu, X. Hao, H. Zhu and J. Min, *Adv. Mater.*, 2022, **34**, 2110147.
13 K. Chong, X. Xu, H. Meng, J. Xue, L. Yu, W. Ma and Q. Peng, *Adv. Mater.*, 2022, **34**, 2109516.
14 P. Bi, S. Zhang, Z. Chen, Y. Xu, Y. Cui, T. Zhang, J. Ren, J. Qin, L. Hong, X. Hao and J. Hou, *Joule*, 2021, **5**, 2408–2419.
15 C. Li, X. Gu, Z. Chen, X. Han, N. Yu, Y. Wei, J. Gao, H. Chen, M. Zhang, A. Wang, J. Zhang, Z. Wei, Q. Peng, Z. Tang, X. Hao, X. Zhang and H. Huang, *J. Am. Chem. Soc.*, 2022, **144**, 14731–14739.
16 C. He, Z. Chen, T. Wang, Z. Shen, Y. Li, J. Zhou, J. Yu, H. Fang, Y. Li, S. Li, X. Lu, W. Ma, F. Gao, Z. Xie, V. Coropceanu, H. Zhu, J.-L. Bredas, L. Zuo and H. Chen, *Nat. Commun.*, 2022, **13**, 2598.
17 L. Zhou, L. Meng, J. Zhang, C. Zhu, S. Qin, I. Angunawela, Y. Wan, H. Ade and Y. Li, *Adv. Funct. Mater.*, 2021, **32**, 2109271.
18 Y. Wei, Z. Chen, G. Lu, N. Yu, C. Li, J. Gao, X. Gu, X. Hao, G. Lu, Z. Tang, J. Zhang, Z. Wei, X. Zhang and H. Huang, *Adv. Mater.*, 2022, **34**, 2204718.
19 X. Zhang, H. Wang, D. Li, M. Chen, Y. Mao, B. Du, Y. Zhuang, W. Tan, W. Huang, Y. Zhao, D. Liu and T. Wang, *Macromolecules*, 2020, **53**, 3747–3755.
20 Y. Xiao, R. Ma, G. Zhou, J. Zhu, T.-K. Lau, S. Dai, J. J. Rech, N. Zhao, W. You, H. Yan, X. Zhan and X. Lu, *ACS Appl. Energy Mater.*, 2020, **3**, 10814–10822.
21 E. E. Greciano, J. Calbo, E. Orti and L. Sanchez, *Angew. Chem.*, 2020, **132**, 17670–17677.
22 T. Zhang, D. B. Dement, V. E. Ferry and R. J. Holmes, *Nat. Commun.*, 2019, **10**, 1156.
23 Q. Guo, Y. Liu, M. Liu, H. Zhang, X. Qian, J. Yang, J. Wang, W. Xue, Q. Zhao, X. Xu, W. Ma, Z. Tang, Y. Li and Z. Bo, *Adv. Mater.*, 2020, **32**, 2003164.
24 X. Lai, H. Lai, M. Du, H. Chen, D. Qiu, Y. Zhu, M. Pu, Y. Zhu, E. Zhou and F. He, *Chem. Mater.*, 2022, **34**, 7886–7896.
25 C. Cao, H. Wang, D. Qiu, T. Zhao, Y. Zhu, X. Lai, M. Pu, Y. Li, H. Li, H. Chen and F. He, *Adv. Funct. Mater.*, 2022, **33**, 2201828.
26 L. Yu, M. Zhang, J. Tang, R. Li, X. Xu and Q. Peng, *Chem. Mater.*, 2021, **33**, 7396–7407.
27 G. Zeng, W. Chen, X. Chen, Y. Hu, Y. Chen, B. Zhang, H. Chen, W. Sun, Y. Shen, Y. Li, F. Yan and Y. Li, *J. Am. Chem. Soc.*, 2022, **144**, 8658–8668.
28 C. Cao, H. Lai, H. Chen, Y. Zhu, M. Pu, N. Zheng and F. He, *J. Mater. Chem. A*, 2021, **9**, 16418.
29 Y. Cui, H. Yao, J. Zhang, K. Xian, T. Zhang, L. Hong, Y. Wang, Y. Xu, K. Ma, C. An, C. He, Z. Wei, F. Gao and J. Hou, *Adv. Mater.*, 2020, **32**, 1908205.
30 C. Li, J. Zhou, J. Song, J. Xu, H. Zhang, X. Zhang, J. Guo, L. Zhu, D. Wei, G. Han, J. Min, Y. Zhang, Z. Xie, Y. Yi, H. Yan, F. Gao, F. Liu and Y. Sun, *Nat. Energy*, 2021, **6**, 605–613.
31 H. Lai, Q. Zhao, Z. Chen, H. Chen, P. Chao, Y. Zhu, Y. Lang, N. Zhen, D. Mo, Y. Zhang and F. He, *Joule*, 2020, **4**, 688–700.
32 X. Shen, X. Lai, H. Lai, T. Zhao, Y. Zhu, M. Pu, H. Wang, P. Tan and F. He, *Macromolecules*, 2022, **55**, 6384–6393.
33 W. Feng, S. Wu, H. Chen, L. Meng, F. Huang, H. Liang, J. Zhang, Z. Wei, X. Wan, C. Li, Z. Yao and Y. Chen, *Adv. Energy Mater.*, 2022, **12**, 2104060.
34 J. Xu, F. Lin, L. Zhu, M. Zhang, T. Hao, G. Zhou, K. Gao, Y. Zou, G. Wei, Y. Yi, A. K. Y. Jen, Y. Zhang and F. Liu, *Adv. Energy Mater.*, 2022, **12**, 2201338.
35 J. Zhang, F. Bai, I. Angunawela, X. Xu, S. Luo, C. Li, G. Chai, H. Yu, Y. Chen, H. Hu, Z. Ma, H. Ade and H. Yan, *Adv. Energy Mater.*, 2021, **11**, 2102596.
36 T. Yu, W. He, M. Jafari, T. Guner, P. Li, M. Siaj, R. Izquierdo, B. Sun, G. C. Welch, A. Yurtsever and D. Ma, *Small Methods*, 2022, **6**, 2100916.

37 K. Jiang, Q. Wei, J. Y. L. Lai, Z. Peng, H. K. Kim, J. Yuan, L. Ye, H. Ade, Y. Zou and H. Yan, *Joule*, 2019, **3**, 3020–3033.
38 P. Tan, L. Liu, Z. Y. Chen, H. Lai, Y. Zhu, H. Chen, N. Zheng, Y. Zhang and F. He, *Adv. Funct. Mater.*, 2021, **31**, 2106524.
39 C. Li, J. Zhou, J. Song, J. Xu, H. Zhang, X. Zhang, J. Guo, L. Zhu, D. Wei, G. Han, J. Min, Y. Zhang, Z. Xie, Y. Yi, H. Yan, F. Gao, F. Liu and Y. Sun, *Nat. Energy*, 2021, **6**, 605–613.
40 D. Mo, H. Chen, J. Zhou, N. Tang, L. Han, Y. Zhu, P. Chao, H. Lai, Z. Xie and F. He, *J. Mater. Chem. A*, 2020, **8**, 8903–8912.
41 X. Li, H. Huang, I. Angunawela, J. Zhou, J. Du, A. Liebman-Pelaez, C. Zhu, Z. Zhang, L. Meng, Z. Xie, H. Ade and Y. Li, *Adv. Funct. Mater.*, 2019, **30**, 1906855.